Journal of Fluorescence (2019) 29:165–176
https://doi.org/10.1007/s10895-018-2324-2

ORIGINAL ARTICLE

Quenching of Luminol Fluorescence at Nano-Bio Interface: Towards the Development of an Efficient Energy Transfer System

Vikash Kumar Sonu [1] · Sivaprasad Mitra [1]

Received: 10 September 2018 / Accepted: 5 November 2018 / Published online: 6 December 2018

Abstract

Surface modified colloidal gold (Au) and silver (Ag) nanoparticles (NPs) were used as efficient quenchers of luminol (LH_2) fluorescence either in homogeneous aqueous medium or its noncovalent assembly with bovine serum albumin (BSA). The mechanism as well as the extent of fluorescence quenching was found to be strongly dependent on the nature of the nanoparticles. While simple static type fluorescence quenching mechanism was perceived with AuNP, a more complex protocol involving quenching sphere model was envisaged for AgNP quenching. Nevertheless, the magnitude of Stern-Volmer (SV) quenching constant ($K_{SV} \sim 10^8$–10^{10} M^{-1}) was calculated to be ca. 10^4 times more for surface quoted NPs in comparison with BSA–NP bioconjugates system. On the other hand, a highly efficient ($E \approx 95\%$) energy transfer (ET) process was predicted for LH_2 captured in the hydrophobic assembly with BSA in presence of AgNP as an acceptor. The ET efficiency is critically dependent on the concentration of BSA and nicely correlated with the extent of NP surface coverage. However, fluorescence quenching on AuNP surface is relatively less responsive towards protein concentration, primarily due to the difference in surface activity as well as the mode of interaction of the protein with NPs.

Keywords Luminol · Metal nanoparticles · Fluorescence quenching · Bovine serum albumin · Energy transfer · Bionanosensors

Introduction

Chemiluminescent (CL) property of luminol (3-aminophthalic hydrazide, LH_2) has wide application in different fields like forensic science, biological and curative science [1–10].

Highlights
- Luminol (LH_2) fluorescence quenches in presence of BSA-nanoparticle (NP) conjugate;
- Fluorescence quenching with AuNP follows simple Stern-Volmer mechanism;
- Quenching sphere mechanism is prevailed in case of AgNP;
- Concentration of BSA controls the energy transfer (ET) efficiency critically;
- ET in LH_2 – BSA – AgNP conjugate can act as potential bionanosensor.

Electronic supplementary material The online version of this article (https://doi.org/10.1007/s10895-018-2324-2) contains supplementary material, which is available to authorized users.

✉ Sivaprasad Mitra
smitranehu@gmail.com; smitra@nehu.ac.in

[1] Centre for Advanced Studies, Department of Chemistry, North-Eastern Hill University, Shillong 793022, India

Literature reports suggest that the CL intensity of LH_2 in H_2O_2 can be boosted by different metal or metal oxide nanoparticles (NPs) including gold/silver alloy and $CoFe_2O_4$ etc. [11–17] and also in presence different organic compounds like glutathione, L-cysteine, N-acetylcysteine and/or biological macromolecules like bovine serum albumin [18–20]. Gold NPs act as catalyst for instantaneous generation of H_2O_2 from dissolved oxygen in luminol-hydrazine system and this sensitive method is used in quantitative determination of hydrazine in boiler feed water [21].

It is already well-known that CL of LH_2-H_2O_2 system is not affected by NP size, but is dependent on its concentration [22]. Chemiluminescence resonance energy transfer (CRET) with metal NP (MNP) as acceptor has application in immunoassays, like DNA and micro-RNA analysis, small molecules detection and cell imaging and used to design optical sensor and analytical methodology [23, 24]. The characteristic property of CL is exactly like that of fluorescence emission. The only difference is that while an appropriate chemical process is involved to excite the electrons in the former, a suitable light source is used in the latter case. Thus, the fluorescence

properties of excited LH_2 and its modulation can also be used effectively to monitor several bio-chemical environments, as indeed observed in number of reports [25, 26].

Molecular properties of organic systems can be functionalized by physical adsorption on MNPs towards desired applications including biomedical sciences [27, 28], antibacterial systems [29], sensing elements [30] as well as drug carriers [31]. Further, the application of MNPs as acceptors in energy transfer (ET) pair has significantly improved the overall efficiency of the process, making it suitable to probe a larger change in macromolecular conformation; which, until now, was not possible to achieve with conventional organic molecules as acceptors. The primary reason for this enhanced sensitivity of ET is attributed to the electromagnetic interaction between the donor dipole and the surface electrons of the NPs [32]. Further, the geometrical restriction in typical D – A pair seems to be irrelevant due to the spherical shape of the acceptor NPs.

On the other hand, extensive literature reports are available on the modification of MNP surface due to adsorption of plasma proteins on it [33]. Immense interest was to probe the bovine serum albumin (BSA) adsorption on different NP surface because of its easy availability in pure form and extraordinary solubility in water. In one of our previous reports it was shown that the conformers **I** and **II** (Fig. 1) contribute significantly towards the fluorescence of LH_2 in aqueous medium [34]. Further, the modulation of fluorescence behavior of LH_2 in presence of a series of sequestering agents including BSA [35] and HSA [36] was also reported. It is evident that while the non-polar fraction of LH_2 (**II**, $\mu = 1.92$ D) binds specifically in subdomain IIA of both the albumins, binding of relatively polar fraction (**I**, $\mu = 2.12$ D) in the other binding domain (IA) of BSA seems important. In the present communication, the modulatory effect of MNPs on LH_2 luminescence was monitored in presence of BSA. The motivation of the work lies in exploring a newer and simple system for developing a more efficient biosensor since both the silver and gold NPs can be easily tagged to different bio-macromolecular architecture.

Experimental Section

Chemicals

Luminol (LH_2, 97%) and lyophilized powder form of BSA were used as received from Sigma-Aldrich Chemical Pvt. Ltd. The details of syntheses and complete characterization of metallic gold and silver nanoparticles (Au and AgNP, respectively) with estimated size of 13 ± 2 and 8 ± 2 nm have been described elsewhere [37]. The surface plasmon resonance (SPR) peaks obtained at 400 and 518 nm for Ag and AuNP respectively are due to the collective oscillation of the free conduction electrons with incident electromagnetic radiation [38]. The concentration of synthesized nanoparticles is ~7.2 and ~2.6 nM for silver and gold, respectively which is calculated according to literature report [39, 40].

Instrumentation and Data Analysis

The experimental protocol and data analysis procedure is same as reported earlier [41, 42]. The steady state fluorescence emission spectra of LH_2 were collected by exciting the sample at 320 nm, where the interference with the NP absorption is least. The emission spectra were corrected for instrument response function as well as from the sample blanks collected at identical condition. Finally, individual fluorescence spectrum (F) of LH_2 in presence of different concentration of protein and/or NP was corrected for any possible repartitioning of the excitation light by using the following relation:

$$F^{corr}\left(\lambda_E\ ,\lambda_F\right) = F\left(\lambda_E\ ,\lambda_F\right) \times \frac{A\ (\lambda_E)}{A_{tot}\ (\lambda_E)} \qquad (1)$$

Where, A represents the absorption of free LH_2 and A_{tot} is the total absorbance of the solution at the excitation wavelength (λ_E). Thus, the final corrected spectrum is considered as the contribution only from LH_2 fluorescence. The results obtained from three distinct set of experiments were averaged and further analyzed using Origin 6.0 (Microcal Software, Inc., USA).

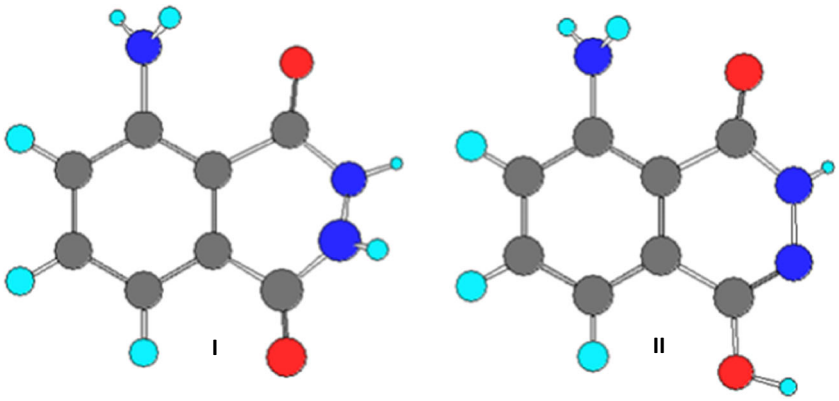

Fig. 1 Primary structural isomers with significant contribution in total fluorescence of luminol (LH_2)

The fluorescence quenching experiment was performed by adding desired amount of quencher into a solution of fixed concentration of LH_2 (~1 μM). The quenching data was analyzed by Stern-Volmer (SV) model (Eqs. 2a and 2b) for both static and dynamic quenching [43].

$$\frac{F_0}{F} = 1 + K_{SV}[Q] = 1 + k_q\tau_0[Q] \tag{2a}$$

$$\frac{\tau_0}{\tau} = 1\ (static); \frac{\tau_0}{\tau} = \frac{F_0}{F}\ (dynamic) \tag{2b}$$

The parameters F_0 (τ_0) and F (τ) indicate the fluorescence intensity (lifetime) in the absence and presence of certain quencher concentration [Q], respectively. K_{SV} is SV quenching constant and κ_q is diffusion controlled bimolecular quenching rate constant.

For the static quenching case, as observed in the present study, K_{SV} is considered as the ground state association constant (K_a) of the fluorophore – quencher pair. Measurement of this quantity at various experimental temperature leads to the evaluation of other thermodynamic parameters for binding using the following set of relations [44]:

$$logK_a = -\frac{\Delta H}{2.303RT} + \frac{\Delta S}{2.303R} \tag{3a}$$

$$\Delta G = \Delta H - T\cdot\Delta S \tag{3b}$$

Considering the presence of similar but independent binding sites as well as an equilibrium between the unbound and the bound, non-fluorescent LH_2 – NP complex, the stoichiometry (n) of binding to the fluorophore can be determined from the LH_2 fluorescence intensity variation data in presence of NP quencher by using Eq. (4) [42].

$$\log\left[\frac{F_0 - F}{F}\right] = logK_a + nlog[NP] \tag{4}$$

Fluorescence decay curves of LH_2 were collected by exciting the sample with 365 nm LED in a picomaster (PM3) time-correlated single photon counting (TCSPC) apparatus (PTI, USA) [37]. The experimentally obtained decay traces F(t) were expressed as a sum of exponentials (Eq. 5) [45].

$$F(t) = \sum_i \alpha_i \exp\left(\frac{-t}{\tau_i}\right) \tag{5}$$

Where, α_i is the amplitude of the i^{th} component associated with lifetime τ_i; such that $\sum\alpha_i = 1$. The average fluorophore lifetime (τ_{av}) was expressed as fractional contribution (f_i) of each decay time (Eq. 6) to the steady state intensity [46].

$$\tau_{av} = \sum_i f_i\tau_i = \frac{\sum_i \alpha_i\tau_i^2}{\sum_i \alpha_i\tau_i} \tag{6}$$

Result and Discussion

Characterizing LH_2 – NP Interaction in Aqueous Buffer Medium

When excited at $S_1(\pi) \leftarrow S_0(\pi)$ absorption ranging within 320–380 nm region, LH_2 gives a strong unstructured and broad emission spectrum within 375–520 nm range with fluorescence yield of 0.72 [34]. LH_2 fluorescence is found to quench extremely efficiently in presence of both Ag and Au NPs (Fig. 2(i)). Interestingly, while the SV analysis of the quenching data gives a straight line for AuNP, it shows an upward curvature for the AgNP (inset, Fig. 2(i)) & Fig. 1S). To confirm the quenching mechanism, time-resolved fluorescence decay measurement of LH_2 was monitored both in absence and presence of the quencher. In aqueous buffer solution, LH_2 fluorescence decay is best described by a two exponential decay function with $\tau_1 = 2.4$ ($a_1 = 24\%$) and $\tau_2 = 9.8$ ns ($a_2 = 76\%$), respectively with an average lifetime of 9.2 ± 0.2 ns [35]. On successive addition of both Ag and Au NPs, the fluorescence decay of LH_2 still remains bi-exponential (Fig. 2S) without significant variation in the average lifetime (inset, Fig. 2(i)), indicating a static type mechanism in both the cases.

In absence of any dynamic or diffusive quenching process, a positive deviation in SV plot in presence of AgNP suggests the situation where the extent of quenching is very high. It may arise due to the development of a quenching sphere [47–49] within which the probability of quenching is almost unity because of efficient non-radiative energy transfer between the excited LH_2 as donor and AgNP as acceptor (see later). The possibility for the quencher to be inside this sphere at the time of excitation depends on the volume (V) and the quencher concentration, [Q]. The overall probability of this extra quenching is introduced into the linear SV equation (Eq. 2a) to give the following relations [50].

$$\frac{F_0}{F} = \{1 + K_{SV}[Q]\} \times e^{V_q\cdot[Q]} \tag{7}$$

$$V_q = N_A \times V = N_A \times \frac{4}{3}\pi R_S^3 \tag{8}$$

Here, K_{SV} is quenching constant defining the linear part of the SV plot and R_S is the radius of quenching sphere.

Simulation results of LH_2 fluorescence quenching data in presence of Ag and AuNP at some representative temperatures are given in Table 1 & Fig. 1S. It is to be noted that the magnitude of K_{SV} is about 2~3 times more for AgNP in comparison with AuNP. The K_{SV} values obtained at different temperature are used to estimate the thermodynamic factors of LH_2-NP interaction. The negative values of ΔG assert that the binding process is spontaneous in the whole temperature range. Further, the higher negative ΔG value for LH_2-AgNP

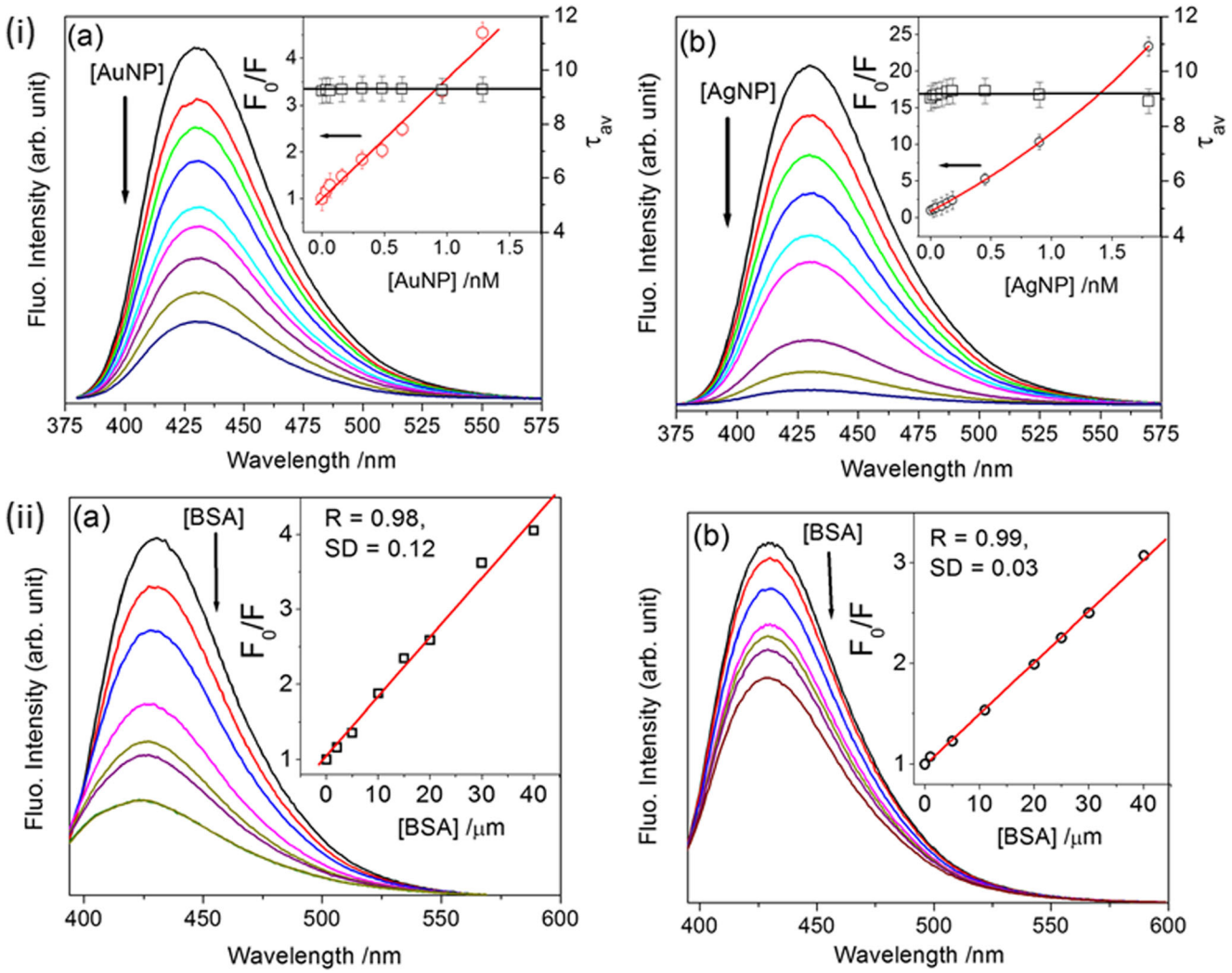

Fig. 2 (i) Quenching of LH_2 fluorescence in presence of varying concentration of Au (a) and Ag (b) NPs. Inset shows the Stern-Volmer analysis of the quenching data (circles) and simulated lines using Eqs. 2a, 2b and 7 for Au and AgNP, respectively. The variation in LH_2 average lifetime (τ_{av}) obtained by using Eq. 6 at each quencher concentration is shown by empty squares in both the cases. (ii) Variation of LH_2 – NP composite fluorescence in presence of varying concentration of BSA. [LH_2] = 1 μM, [AgNP] = [AuNP] = 0.32 nM (b), [BSA] = 0 ~ 40 μM (along the arrow direction) in each case. Inset shows the SV plot obtained from the respective quenching data

Table 1 Thermodynamic and other binding parameters corresponding to the interaction of LH_2 with Ag and AuNP

Temp. (K)	AuNP				AgNP					
	K_{SV} /10^9, M^{-1}	ΔH	ΔS	ΔG	K_{SV} /10^9	ΔH	ΔS	ΔG	V_q /10^8, cm^3	R_S, nm
298	2.56 ± 0.12	8.16	207.60	−53.70	8.50 ± 0.22	9.60	222.24	−56.62	2.01 ± 0.13	43.0
303	2.77 ± 0.11			−54.74	9.05 ± 0.25			−57.73	1.87 ± 0.14	42.0
308	2.88 ± 0.14			−55.78	9.56 ± 0.26			−58.85	1.85 ± 0.14	41.8
313	2.98 ± 0.13			−56.82	9.47 ± 0.42			−59.96	2.51 ± 0.23	46.3
318	3.15 ± 0.14			−57.86	10.69 ± 0.14			−61.07	2.35 ± 0.24	45.3
323	3.36 ± 0.15			−58.89	11.75 ± 0.50			−62.18	2.07 ± 0.22	43.4

K_{SV} values are obtained from Eqs. (2a) and (7) for AuNp and AgNP, respectively, the error limit indicates the confidence interval in three independent measurements (mean ± S.D.). ΔH and ΔG are represented in kJ mol^{-1} ; whereas, ΔS is in J K^{-1} mol^{-1}

complex in comparison with LH_2-AuNP system is consistent with the assumption of stronger interaction in the former (see below). In both the cases, the magnitude of ΔH is positive. Therefore, the spontaneous adsorption process is mainly governed by the overall positive entropy change during binding. Due to inherent complexity of the investigated systems and difference in quenching mechanism for Au and Ag NP system discussed above, the calculation of binding stoichiometry in these cases is not straightforward. Nevertheless, analysis of LH_2 fluorescence quenching data using double-log plot (Eq. 4), shown in Fig. 3S, reveals that while the apparent stoichiometry of binding is 1:1 for LH_2–AgNP system, the corresponding ratio is estimated to be 3:2 for LH_2–AuNP system. Higher K_{SV} values along with a positively deviated SV plot gives clear indication about relatively stronger interaction in the former. This result is consistent with higher reactivity and can be correlated with excess charge density (smaller size) of AgNP in contrast with AuNP (see below) [51].

As mentioned earlier, the fluorescence decay data of LH_2 still remains bi-exponential in the whole concentration range of added NPs. The fast and slow decay components, corresponding to structures **I** and **II** (Fig. 1), contributes approximately in 1:3 ratio towards the total LH_2 fluorescence [35]. However, interesting observation on the fractional contribution of each component is seen upon global analysis of whole data set in presence of NPs (Table 1S). In both the cases, the contribution of fast decay component decreases significantly (~25%) on addition of NPs indicating that LH_2 preferentially binds with MNP surfaces with structure **I** and therefore, results the decrease in overall fluorescence intensity (quenching). The preferential binding of the NPs with conformer **I** seems justified from the structural point of view of this conformer in comparison with its counterpart, **II** (Fig. 1). The two adjacent amino groups in conformer **I** are suitably located to make a tweezer shaped anchor on the spherical NP surface in comparison with asymmetric distribution of binding regions in isomeric structure **II**.

Binding of LH_2 – NP Composite with Bovine Serum Albumin (BSA)

Fluorescence intensity of LH_2 is known to be quenched in presence of BSA due to the sequestration of the probe in subdomains IA and IIA of the protein with positive cooperativity [35]. The static type quenching till ~30 μM BSA concentration over different temperature range was characterized with moderately high binding constant ($2.4 \pm 0.1 \times 10^5$ M^{-1}). Interestingly, fluorescence intensity of LH_2 adsorbed on MNP surface (hereinafter referred as LH_2 – NP conjugate) also quenches regularly in presence BSA (Fig. 2(ii)). However, in contrast to the free LH_2 fluorescence spectral shift of ~10 nm [35], LH_2 – NP conjugate shows a blue shift of only about 5 and 3 nm (for AgNP and AuNP, respectively) on binding with BSA. Therefore, it is believed that the association of LH_2 adsorbed on NP surface in protein binding domain (PBD) is not as efficient as in case of free LH_2. The quenching of LH_2 – NP fluorescence follows linear SV relationship (inset of Fig. 2(ii)) and the corresponding parameters are listed in supplementary section (Table 2S). As expected, the magnitude of K_{SV} is little higher in case of LH_2 – AgNP in comparison with LH_2 - AuNP system. However, in both the cases, it is about an order of magnitude less while comparing with free LH_2 fluorescence quenching by BSA [35].

The existence of cooperativity in the binding of small molecules on macromolecular protein surfaces can be confirmed by Hill analysis (Eq. 9); where, ΔF (= $F_0 - F$) is the change in fluorescence intensity of LH_2–NP conjugate in presence of substrate [S], and ΔF_{max} is the maximum change in fluorescence intensity, $K_{0.5}$ is the concentration of BSA that brings half maximal fluorescence change and the Hill parameter (n_H) represents the degree of cooperativity in the association process. For $n_H > 1$, the situation is described by positive cooperativity, i.e. once the protein molecule is bound to the NP, its affinity to NP increases further. For $n_H < 1$, the binding strength of the protein to the NP becomes gradually weaker (negatively cooperative). Finally, for a non-cooperative association, the magnitude of $n_H = 1$ [35]. The protein – NP interaction is believed to follow the assumptions of Langmuir adsorption isotherm [52].

$$\frac{\Delta F}{\Delta F_{max}} = \frac{[S]^{n_H}}{K_{0.5}^{n_H} + [S]^{n_H}} \tag{9}$$

For example, LH_2 interacts with two PBDs of BSA (subdomains IA and IIA) with n_H and $K_{0.5}$ values of 2.2 and 6.0 μM, respectively [35]. Interestingly, the magnitude of n_H for the interaction of LH_2 – NP conjugates in presence of BSA are found to be significantly lower (ca. 1.3 ~ 1.7) at different temperatures (Fig. 3(i) and Table 2S). Further, $K_{0.5}$ is significantly higher (7~10 μM) in the present case. These results indicate relatively less efficient binding of the protein with LH_2 – NP composite system and may signify the importance of nano-toxicity on the activity of serum albumins as carrier protein [53, 54].

TCSPC analyses of LH_2-NP-BSA ternary systems show certain interesting features (Fig. 4). The total contribution of component **I** increase by ca. 25% at 40 μM protein, presumably due to the disruption of weak **I** – AuNP interaction discussed in the preceding section and subsequent release of certain fraction of **I** in the solution. However, for AgNP, the situation is far more complex and interesting. Along with the two decay components mentioned above, an additional 0.67 ns component appears with significant contribution (>10%) in presence of even only 1 μM BSA. The contribution of this component increases continuously and reaches ca. 80%

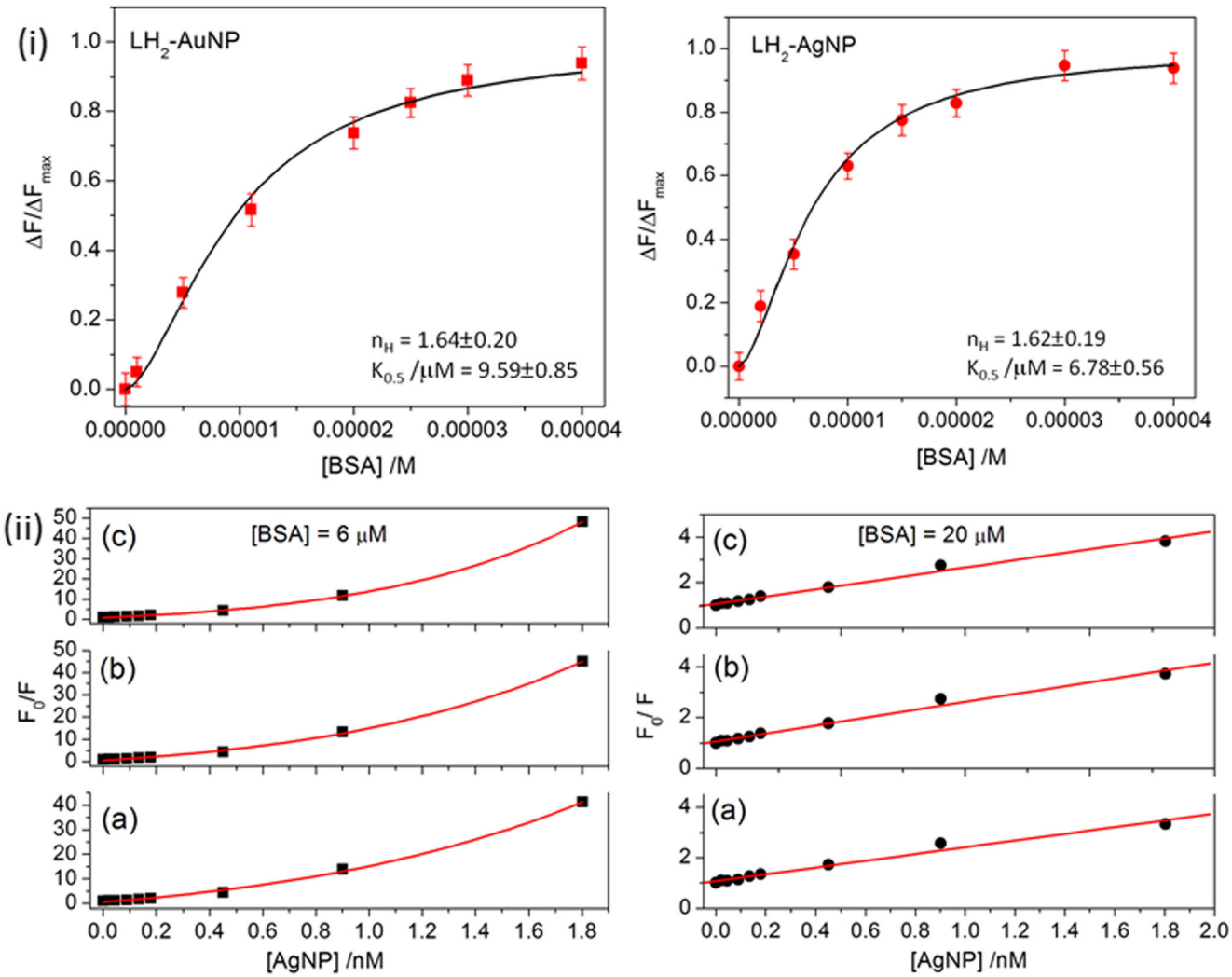

Fig. 3 (i) Representative Hill plots for LH_2 – NP – BSA system at 298 K. The solid line indicates the simulation of experimental data points using Eq. (9). The corresponding parameters obtained from the fitting result are also shown. (ii) Stern-Volmer analysis for the fluorescence quenching data of LH_2 – BSA assembly in presence of AgNP at 298 K (a), 308 K (b) and 318 K (c). The solid lines represent the simulation of experimental data at [BSA] = 6 (square) and 20 μM (circle) by using Eqs. (7) and (2a), respectively

in 40 μM protein concentration (Fig. 4b). The presence of a fast instrument limited (<100 ps) decay component for free LH_2 in presence of HSA was reported earlier to be due to the formation of "fluorophore-quencher" pair [36]. A similar mechanism can also be envisaged for LH_2 - AgNP system with characteristic decay time of 0.67 ns. However, the absence of any dark complex formation in case of LH_2 – AuNP system indicates that either or both fluorophore/quencher pair is shielded from each other while adsorbed on MNP surface, which results a lesser degree of interaction among them. This is consistent with comparatively lower value K_{SV} as well as less fluorescence spectral blue shift of LH_2 – AuNP system in presence of BSA while comparing with LH_2 – AgNP conjugate discussed before.

The quenching of LH_2 – NP composite system in presence of BSA is consistent with one site binding model ($n = 0.9 \pm 0.1$) with almost similar magnitude of ΔG (Table 2S) for both Ag and AuNP. However, the negative value of ΔH and positive ΔS is observed in case of LH_2 – AuNP; in contrast, the binding of LH_2 – AgNP in BSA is associated with negative ΔS value. Therefore, a combination of van der Waals interaction and hydrogen bond formation also contribute in the overall enthalpy driven process in this case. These results suggest that LH_2 adsorbed on different metal surfaces interact differently with BSA. The difference in physical, chemical and optical behavior of organic fluorophores adsorbed on Ag and AuNP surfaces are well known [55]. For example, aromatic organothiol compounds react with AgNP to form the deprotonated core-shell RS-Ag complex possibly due to its preferential interaction with silver oxide either present or generated in-situ on AgNP surface and the mechanism of interaction of these compounds is significantly different on AgNP in

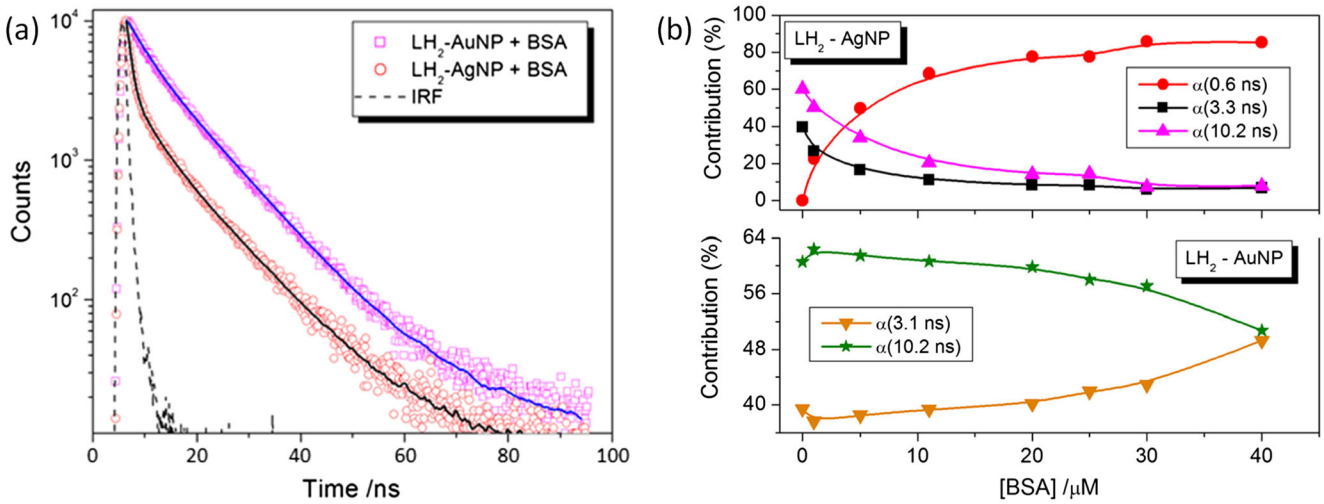

Fig. 4 Time-resolved fluorescence decay (scattered points) and simulated data (solid line) of LH_2 – NP composite system in presence of 20 μM BSA. Instrument response function (IRF) is also shown by dashed line

comparison with AuNP surface [56, 57]. A similar behavior may explain the difference in the experimental results observed here in case of AgNP from that in the relatively idealized AuNP surface.

Quenching of LH_2 Fluorescence Bound Inside BSA Cavity by MNPs

On the other hand, it is interesting to verify the interaction behavior of LH_2 – BSA assembly with spherical MNPs. Effect of addition of both Ag and AuNP on LH_2 fluorescence was checked with the incubated solution of BSA at two different concentration range, viz. 6 and 20 μM. The fluorophore intensity was found to decrease regularly with the addition of NPs. It is interesting to note that while the analysis of the quenching data is consistent with linear S-V plot in presence of 20 μM BSA as shown in Fig. 3(ii), a sharp upward curvature is observed for the quenching of LH_2 with AgNP in presence of 6 μM BSA. All the characteristic data calculated from SV analysis for each of the systems is given in Tables 2 and 3.

Calculation of thermodynamic parameters in different LH_2 – BSA – NP systems indicate that interaction is principally hydrophobic in nature in all the cases, except for AgNP in presence of 6 μM BSA. In this case, along with the structural distortion of the protein environment with positive entropy change for the binding, van der Waals interaction as well as possible hydrogen bond formation may also be important. Also, the difference in the nature of van't Hoff plot for the interaction of AgNP with aqueous LH_2 and LH_2 – BSA assembly (Fig. 4S) signifies the specific role of BSA in the interaction process.

The data analyzed by quenching-sphere model for LH_2 – BSA (6 μM) fluorescence intensity diminution in presence of AgNP reveals certain interesting observations. While, the calculated values of R_S are ~ 43 ± 3 nm at different temperatures for AgNP in absence of albumin, the corresponding value is ca. ~ 65 ± 5 nm in presence of 6 μM BSA. Therefore, it can be concluded that BSA has specific role in bringing the fluorophore quencher pair in close vicinity of each other. However, as we do not see any additional quenching

Table 2 Thermodynamic and other binding parameters corresponding to the interaction of LH_2 incubated in 6 μM BSA with Ag and AuNP

Temp. (K)	AuNP				AgNP					
	K_{SV} /10^9, M^{-1}	ΔH	ΔS	ΔG	K_{SV} /10^9	ΔH	ΔS	ΔG	V_q /10^8, cm^3	R_S, nm
298	1.61 ± 0.11	10.84	212.70	−52.55	8.00 ± 0.90	−20.9	119.71	−56.55	5.50 ± 0.60	60.2
303	1.76 ± 0.11			−53.61	7.14 ± 0.70			−57.15	6.36 ± 0.54	63.2
308	1.86 ± 0.11			−54.67	6.74 ± 0.68			−57.75	6.87 ± 0.51	64.9
313	2.00 ± 0.10			−55.74	5.09 ± 0.31			−58.35	8.60 ± 0.30	69.9
318	2.12 ± 0.09			−56.80	4.59 ± 0.18			−58.95	9.18 ± 0.19	71.4
323	2.28 ± 0.10			−57.86	4.43 ± 0.16			−59.54	9.24 ± 0.18	71.5

K_{SV} values are obtained from Eqs. (2a) and (7) for AuNp and AgNP, respectively. The error limit indicates the confidence interval in three independent measurements (mean ± S.D.). ΔH and ΔG are represented in kJ mol^{-1}; whereas, ΔS is in J K^{-1} mol^{-1}

Table 3 Thermodynamic and other binding parameters corresponding to the interaction of LH_2 incubated in 20 μM BSA with Ag and AuNP

Temp. (K)	AuNP				AgNP			
	K_{SV} /10^9, M^{-1}	ΔH	ΔS	ΔG	K_{SV} /10^9, M^{-1}	ΔH	ΔS	ΔG
298	1.52 ± 0.11	6.06	196.19	−52.41	1.34 ± 0.08	5.78	194.49	−52.17
303	1.60 ± 0.12			−53.39	1.47 ± 0.07			−53.15
308	1.65 ± 0.13			−54.37	1.55 ± 0.07			−54.12
313	1.72 ± 0.12			−55.35	1.61 ± 0.06			−55.09
318	1.79 ± 0.12			−56.33	1.60 ± 0.07			−56.06
323	1.85 ± 0.12			−57.31	1.62 ± 0.07			−57.04

K_{SV} values are obtained from Eqs. (2a) and (7) for AuNp and AgNP, respectively. The error limit indicates the confidence interval in three independent measurements (mean ± S.D.). ΔH and ΔG are represented in kJ mol^{-1}; whereas, ΔS is in J K^{-1} mol^{-1}

phenomenon (except normal static quenching process resulting in linear SV plot) even in presence of 20 μM BSA concentration, the stoichiometry of the LH_2 – BSA – AgNP assembly system seems to be a critical factor (see below).

Time resolved measurements were done at each NP addition into LH_2 - BSA systems. The results are almost similar to those described in the previous section. In brief, quenching of LH_2 – BSA bio-conjugate system only in presence of AgNP at both the protein concentration results the formation of an additional fast decay component of 0.5 ± 0.1 ns. This is in sharp contrast to the AuNP case, where the decay follows the usual bi-exponential function always (Table 3S).

LH_2 – NP Assembly as a Super-Efficient Energy Transfer System in Presence of BSA

Very high K_{SV} values either in absence or presence of BSA (Tables 1 and 2) indicate that the quenching process is an efficient non-radiative energy transfer (ET) from LH_2 to the MNPs [58]. Since the dimensions of the NPs for the present study varies within 8~13 nm, the quenching phenomenon predominates over plasmonic near-field augmentation, which is reported for extremely small sized NPs [59, 60].

In the framework of Förster's theory [61], the dipole induced ET efficiency (E) is related with the distance (r) between the donor (D) – acceptor (A) pair as

$$E = 1 - \frac{F}{F_0} = \frac{1}{1 + \left(\frac{r}{R_0}\right)^6} \tag{10}$$

R_0 is the critical Förster distance, defined as the distance where 50% energy transfer efficiency is achieved, and can be expressed as

$$R_0(\text{Å}) = 0.211[\kappa^2 n^{-4} \phi_D J(\lambda)]^{1/6} \tag{11}$$

where, n is the refractive index of the medium and usually taken as 1.36 for aqueous buffer solution [62]. Fluorescence yield (ϕ_D) of donor LH_2 is calculated to be 0.78 in aqueous buffer; whereas, the corresponding values in presence of 6 and 20 μM BSA are 0.59 and 0.32, respectively. The overlap integral J(λ) represents the degree of spectral overlap (shown in Fig. 5) between D and A molecules, and can be expressed as

$$J(\lambda) = \frac{\int_0^\alpha F_D(\lambda)\varepsilon_A(\lambda)\lambda^4 d\lambda}{\int_0^\alpha F_D(\lambda) d\lambda} \tag{12}$$

$F_D(\lambda)$ is the fluorescence intensity of D in the wavelength range of λ to λ + dλ and is dimensionless, $\varepsilon_A(\lambda)$ is the molar absorptivity (in dm^3 mol^{-1} cm^{-1}) of A at wavelength λ. In Eq. 11, κ^2 represent a factor describing the relative orientation of D and A; and usually taken as 2/3 considering the random distribution.

The calculated values of ET parameters in several systems are displayed in Table 4. The average distance between the donor – acceptor pairs in all the cases fall within the range of $0.5R_0 < r < 1.5R_0$, that indicates a highly efficient energy

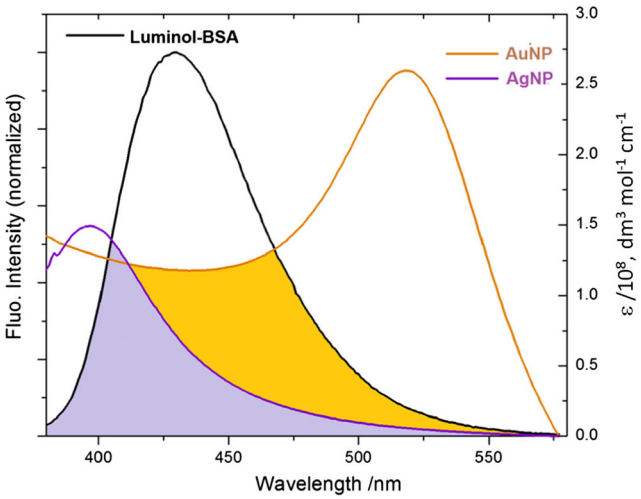

Fig. 5 Spectral overlap (shaded portion) between the fluorescence of LH_2 – BSA (6 μM) and the absorption of Au and Ag NP. The calculated ET parameters are shown in Table 4

Table 4 Calculated values of energy transfer efficiency (E), overlap integral (J), critical Förster's distance (R_0) and donor (D) – acceptor (A) distance (r) for several D – A combinations

Donor	Acceptor	E	J, /10^{18} dm^3 mol^{-1} cm^{-1} nm^4	R_0, /Å	r, /nm
LH_2	AuNP	0.78	9.57894	224.742	18.20
LH_2	AgNP	0.54	2.11658	174.745	17.06
LH_2 – BSA (6 μM)	AuNP	0.69	9.62408	214.693	18.79
LH_2 – BSA (6 μM)	AgNP	0.97	2.12779	166.947	9.35
LH_2 – BSA (20 μM)	AuNP	0.55	9.5245	193.545	18.76
LH_2 – BSA (20 μM)	AgNP	0.66	2.1849	151.430	13.59

transfer between LH_2 donor and the NP acceptors [63, 64]. Further, it is apparently clear from Table 4 that although the R_0 values are higher for AuNP in all the cases, the energy transfer efficiency is always greater for AgNP system. Therefore, it can be argued that although AuNP can induce as an acceptor from a longer distance, AgNP forms more efficient donor-acceptor pair with either LH_2 or hydrophobic assembly of LH_2 – BSA system. This is presumably due to high molar absorptivity of the acceptor in the latter case. The molar absorptivity of spherical Ag and Au NPs with diameter 'd' (in nm) can be estimated from the following empirical relationship [65].

$$\epsilon_{max} = A \times d^{\gamma} \tag{13}$$

The adjustable parameters 'A' and 'γ' are found to be ranging within 4.7×10^4 M^{-1} cm^{-1}, 3.30 and 2.3×10^5 M^{-1} cm^{-1}, 3.48 for AuNP ($d \leq 85$ nm) and AgNP ($d \leq 38$ nm), respectively. From the known sizes of the synthesized NPs, the calculated ε_{max} was found to be at least one and half times higher for AgNP.

The calculated value of r (Table 4) for different combination of FRET pair is in qualitative agreement with the structural features of individual components and signifies the importance of BSA in forming a super- efficient ET system. Direct adsorption of LH_2 (donor) on the coated NP forms a simple D-spacer-A system with an average distance of 17 ± 1 nm. However, in presence of BSA, the situation is more complex and works differently in case of different NPs. On incubation, LH_2 binds preferentially into subdomain IIA of albumin mainly through hydrophobic interaction [35, 36]. On addition of NPs to this assembly, a strong layer of "protein corona" is formed due to preferential adsorption of BSA on the NP surface [66–68]. It is interesting to note here that while BSA is adsorbed "head-on" through a carboxylate – ammonia type salt bridge on citrate stabilized AuNP [69], the interaction with AgNP involves massive deformation in protein secondary structure [70, 71] with possible hysteresis effect on BSA adsorption [72]. Resonance light scattering experiment further suggests that adsorption of BSA on AgNP induces the formation of an aggregate of increased size than the individual BSA molecule [73].

The observation described in the preceding sections of the present investigation can be justified with the structural difference among different nanobioconjugate systems described above. For example, with addition of AuNP in LH_2 – BSA systems produces a soft protein corona which has relatively large D – A distance (with decreased ET efficiency) than free LH_2 – AuNP interaction. However, the structural deformation in BSA and aggregate formation in BSA – AgNP assembly brings the D and A in optimally close to each other resulting significant increase in ET efficiency. However, drastic decrease in ET efficiency at higher BSA concentration (ca. 20 μM) even in presence of AgNP needs further justification. Earlier, it has been shown that adsorption of BSA on AgNP surface gets saturated at [BSA]/[AgNP] ≈ 1 [72]. Considering the dimension of BSA to be (5.5 × 5.5 × 9) nm, a rough estimation on the number of protein molecules adsorbed on a ~10 nm NP surface yields about 3.3×10^{12} molecules/cm^2 for "head on" adsorption and 2.0×10^{12} molecules/cm^2 for "side on" adsorption (in Au and AgNP, respectively) [74, 75]. In the current experimental condition, the situation is arrived when [BSA] is close to ca. 4.50 μM. However, at concentration near 20 μM, random distribution of excess BSA molecules in the solution leads to increase the separation between the donor (LH_2) and acceptor (AgNP) and reduces the ET efficiency.

Recent studies report the ET from an excited fluorophore adsorbed on MNP surface as nanoparticle surface energy transfer (NSET) and propose r^{-4} dependence of ET efficiency. Within this model, the value of R_0 can be calculated independently using Persson-Lang relation (Eq. 14).

$$R_0 = \left(\frac{0.225 c^3 \phi_D}{\omega_D^2 \omega_F \kappa_F} \right)^{1/4} \tag{14}$$

Where, ϕ_D and ω_D are the fluorescence yield and angular frequency of D, ω_F and κ_F are the angular frequency and Fermi wave vector for the NPs. From the known values of ω_F and κ_F for bulk gold (8.4×10^{15} s^{-1} and 1.2×10^8 cm^{-1}, respectively [76, 77], the R_0 values for LH_2 – AuNP and LH_2 – BSA (6 and 20 μM) – AuNP bioconjugates systems are estimated to be 8.66, 8.08 and 6.93 nm, respectively. These values are far below than even the size of the synthesized AuNP (13 ± 2 nm). Therefore, the energy transfer in these systems is more likely to occur via FRET mechanism rather than NSET.

Conclusions

The present investigation reports the interaction of silver and gold nanoparticles (NPs) with fluorescent luminol (LH_2) or non-covalent assembly of LH_2 – BSA system. The values of the Stern-Volmer constant ($K_{SV} \sim 10^9\ M^{-1}$) determined from the fluorescence quenching data in the presence of colloidal NPs are very high in comparison with normal photochemical quenching processes and can be explained based on efficient energy transfer (ET) from LH_2 to NPs. The mechanism as well as the efficiency of ET are significantly different for different NPs and depend critically on the concentration of BSA. The most efficient ET occurs for an LH_2 – BSA (6 μM) non-covalent assembly system with AgNP as acceptor, possibly due to the "side-on" adsorption of the protein onto NP surface; and therefore, bringing the donor – acceptor pair significantly close to each other, in sharp contrast to the relatively soft protein corona formation due to "head-on" adsorption on AuNP. Such energy transfer between confined LH_2 in protein nanocavities and AgNP could lead towards designing new optical-based materials for the application in chemical sensing or light harvesting system. Since LH_2 is known to be an extrmeley efficient chemiluminescent material, bioconjugate systems involving LH_2 – BSA - AgNP nanoassemblies can be developed as efficient chemiluminescence resonance energy transfer (CRET) based bionanosensors for their potential applications.

Acknowledgements The authros acknowledge the support from the Department of Science & Technology (DST), Govt. of India to the Chemistry Department through FIST program (SR/FST/CSI-194/2008).

References

1. Arruda-Vasconcelos R, Chantre RLGF, Lopes RSC, Lopes CC, Barbosa-Ribeiro M, Gomes BPFA (2017) Application of forensic luminol for blood detection in endodontic files. Rev Odontol UNESP 46:227–231. https://doi.org/10.1590/1807-2577.24916
2. Li X, Liu H, He X, Song Z (2010) Determination of cytochrome *c* in human serum and pharmaceutical injections using flow injection chemiluminescence. Appl Biochem Biotechnol 160(4):1065–1073
3. Tan X, Song Z (2014) Human saliva-based quantitative monitoring of clarithromycin by flow injection chemiluminescence analysis: a pharmacokinetic study. Appl Biochem Biotechnol 172(3):1320–1331
4. Liu C, Li B (2011) Silver nanoparticle-initiated chemiluminescence reaction of luminol–$AgNO_3$ and its analytical application. Anal Bioanal Chem 401(1):229–235
5. Gross AM, Harris KA, Kaldun GL (1999) The effect of luminol on presumptive tests and DNA analysis using the polymerase chain reaction. J Forensic Sci 44(4):837–840
6. Khan P, Idrees D, Moxley MA, Corbett JA, Ahmad F, von Figura G, Sly WS, Waheed A, Hassan MI (2014) Luminol-based chemiluminescent signals: clinical and non-clinical application and future uses. Appl Biochem Biotechnol 173(2):333–355
7. Karube I, Yano K, Sasaki S, Nomura Y, Ikebukuro K (2006) Biosensors for environmental monitoring. Ann N Y Acad Sci 864:23–36
8. Wendler J, Hoffmann A, Gross G, Weich HA, Bilitewski U (2005) Development of an enzyme-linked immunoreceptor assay (ELIRA) for quantification of the biological activity of recombinant human bone morphogenetic protein-2. J Biotechnol 119(4):425–435
9. Stockwell BR, Haggarty SJ, Schreiber SL (1999) High-throughput screening of small molecules in miniaturized mammalian cell-based assays involving post-translational modifications. Chem Biol 6(2):71–83
10. Wang Z, Duan N, Li J, Ye J, Ma S, Le G (2011) Ultrasensitive chemiluminescent immunoassay of *Salmonella* with silver enhancement of nanogold labels. Luminescence 26(2):136–141
11. Guo JZ, Cui H, Zhou W, Wang W (2008) Ag nanoparticle-catalyzed chemiluminescent reaction between luminol and hydrogen peroxide. J Photochem Photobiol A Chem 193(2–3):89–96
12. Chen H, Gao F, He R, Cui D (2007) Chemiluminescence of luminol catalyzed by silver nanoparticles. J Colloid Interface Sci 315(1): 158–163
13. Karabchevsky A, Mosayyebi A, Kavokin AV (2016) Tuning the chemiluminescence of a luminol flow using plasmonic nanoparticles. Light Sci Appl 5:e16164. https://doi.org/10.1038/lsa.2016.164
14. Xu SL, Cui H (2007) Luminol chemiluminescence catalysed by colloidal platinum nanoparticles. Luminescence 22(2):77–87
15. Li SF, Zhang XM, Du WX, Ni YH, Wei XW (2008) Chemiluminescence reactions of a luminol system catalyzed by ZnO nanoparticles. J Phys Chem C 113(3):1046–1051
16. Triantis TM, Papadopoulos K, Yannakopoulou E, Dimotikali D, Hrbáč J, Zbořil R (2008) Sensitized chemiluminescence of luminol catalyzed by colloidal dispersions of nanometer-sized ferric oxides. Chem Eng J 144(3):483–488
17. He S, Shi W, Zhang X, Li J, Huang Y (2010) *β*–cyclodextrins-based inclusion complexes of $CoFe_2O_4$magnetic nanoparticles as catalyst for the luminol chemiluminescence system and their applications in hydrogen peroxide detection. Talanta 82(1):377–383
18. Li B, Wang D, Lv J, Zhang Z (2006) Flow-injection chemiluminescence simultaneous determination of cobalt(II) and copper(II) using partial least squares calibration. Talanta 69(1):160–165
19. Du J, Li Y, Lu J (2001) Investigation on the chemiluminescence reaction of luminol–H_2O_2–S^{2-}/R–SH system. Anal Chim Acta 448(1–2):79–83
20. Karatani H et al (1987) Microenvironmental effects of water-soluble polymers on the chemiluminescence of luminol and its analogs. Bull Chem Soc Jpn 60(6):2023–2029
21. Safavi A, Absalan G, Bamdad F (2008) Effect of gold nanoparticle as a novel nanocatalyst on luminol–hydrazine chemiluminescence system and its analytical application. Anal Chim Acta 610(2):243–248
22. Tsogas GZ, Giokas DL, Vlessidis AG (2014) Ultratrace determination of silver, gold, and iron oxide nanoparticles by micelle mediated Preconcentration/selective back-extraction coupled with flow injection chemiluminescence detection. Anal Chem 86(7):3484–3492
23. Huang X, Ren J (2011) Gold nanoparticles based chemiluminescent resonance energy transfer for immunoassay of alpha fetoprotein cancer marker. Anal Chim Acta 686(1–2):115–120
24. Huang X, Ren J (2012) Nanomaterial-based chemiluminescence resonance energy transfer: a strategy to develop new analytical methods. Trends Anal Chem 40:77–89
25. Wang W, Xiong T, Cui H (2008) Fluorescence and electrochemiluminescence of luminol-reduced gold nanoparticles: photostability and platform effect. Langmuir 24(6):2826–2833

26. Komatsu T, Ohira M, Yamada M, Suzuki S (1986) Analytical use of luminescence induced ultrasonically in solution. I. Sonic chemiluminescence of luminol for determination of cobalt(II) at sub-pg levels by flow injection and continuous flow methods. Bull Chem Soc Jpn 59(6):1849–1855
27. Niemeyer CM et al (2001) Nanoparticles, proteins, and nucleic acids: biotechnology meets materials science. Angew Chem Int Ed 40:4128–4158
28. Rosi NL, Mirkin CA (2005) Nanostructures in Biodiagnostics. Chem Rev 105(4):1547–1562
29. Hajipour MJ, Fromm KM, Ashkarran AA, de Aberasturi DJ, de Larramendi IR, Rojo T, Serpooshan V, Parak WJ, Mahmoudi M (2012) Antibacterial properties of nanoparticles. Trends Biotechnol 30(10):499–511
30. Upadhyayula VK et al (2012) Functionalized gold nanoparticle supported sensory mechanisms applied in detection of chemical and biological threat agents: a review. Anal Chim Acta 715:1–18
31. Agasti SS, Rana S, Park MH, Kim CK, You CC, Rotello VM (2010) Nanoparticles for detection and diagnosis. Adv Drug Deliv Rev 62(3):316–328
32. Chatterjee S, Lee JB, Valappil NV, Luo D, Menon VM (2011) Investigating the distance limit of a metal nanoparticle based spectroscopic ruler. Biomed Opt Express 2(6):1727–1733
33. Hao C, Xu G, Feng Y, Lu L, Sun W, Sun R (2017) Fluorescence quenching study on the interaction of ferroferric oxide nanoparticles with bovine serum albumin. Spectrochim Acta A Mol Biomol Spectrosc 184:191–197
34. Moyon NS, Chandra AK, Mitra S (2010) Effect of solvent hydrogen bonding on excited-state properties of Luminol: a combined fluorescence and DFT study. J Phys Chem A 114(1):60–67
35. Moyon NS, Mitra S (2011) Luminol fluorescence quenching in biomimicking environments: sequestration of fluorophore in hydrophobic domain. J Phys Chem B 115(33):10163–10172
36. Moyon NS, Mitra S (2010) On the interaction of luminol with human serum albumin: nature and thermodynamics of ligand binding. Chem Phys Lett 498(1–3):178–183
37. Sonu VK, Islam MM, Rohman MA, Mitra S (2016) Lysozyme binding ability toward psychoactive stimulant drugs: modulatory effect of colloidal metal nanoparticles. Colloids Surf B 146(1):514–522
38. Ghosh SK, Pal T (2007) Interparticle coupling effect on the surface plasmon resonance of gold nanoparticles: from theory to applications. Chem Rev 107(11):4797–4862
39. Sonu VK, Rajkumar I, Bhattacharjee K, Joshi SR, Mitra S (2018) Interaction of caffeine and sulfadiazine with lysozyme adsorbed at colloidal metal nanoparticle interface: influence on drug transport ability and antibacterial activity. J Biomol Struct Dyn. In press. https://doi.org/10.1080/07391102.2018.1426497
40. Haiss W, Thanh NT, Aveyard J, Fernig DG (2007) Determination of size and concentration of gold nanoparticles from UV−Vis spectra. Anal Chem 79(11):4215–4221
41. Phukan S, Mitra S (2012) Fluorescence behavior of ethidium bromide in homogeneous solvents and in presence of bile acid hosts. J Photochem Photobiol A Chem 244:9–17
42. Islam MM, Sonu VK, Gashnga PM, Moyon NS, Mitra S (2016) Caffeine and sulfadiazine interact differently with human serum albumin: a combined fluorescence and molecular docking study. Spectrochim Acta A Mol Biomol Spectrosc 152:23–33
43. Valeur B, Berberan-Santos MN (2012) In: Molecular fluorescence: principles and applications, 2nd edn. Wiley-VCH, Verlag GmbH
44. Silby RJ, Alberty RA (2002) In: Physical chemistry, 3rd edn. John Wiley & Sons (Asia) Pte. Ltd. Singapore
45. Bevington PR, Robinson DK (2003) In: data reduction and error analysis for the physical sciences, 3rd edn. McGraw-Hill, NY
46. Lakowicz JR et al (2006) In: Principles of fluorescence spectroscopy, 3rd edn. Springer, Singapore, Ch. 4
47. Eftink MR, Ghiron CA (1976) Fluorescence quenching of indole and model micelle systems. J Phys Chem 80(5):486–493
48. Jin B, Min KS, Han SW, Kim SK (2009) DNA-binding geometry dependent energy transfer from 4′,6-diamidino-2-phenylindole to cationic porphyrins. Biophys Chem 144(1–2):38–45
49. Castanho MARB, Prieto MJE (1998) Fluorescence quenching data interpretation in biological systems: the use of microscopic models for data analysis and interpretation of complex systems. Biochim Biophys Acta 1373:1–16
50. Airinei A, Tigoianu RI, Rusu E, Dorohoi DO (2011) Fluorescence quenching of anthracene by nitroaromatic compounds. Dig J Nanomater Biostruct 6(3):1265–1272
51. Su Y, Xie Y, Hou X, Lv Y (2014) Recent advances in analytical applications of Nanomaterials in liquid-phase Chemiluminescence. Appl Spectrosc Rev 49(3):201–232
52. Chatterjee T, Mukherjee D, Dey S, Pal A, Hoque KM, Chakrabarti P (2011) Accessory cholera enterotoxin, ace, from vibrio cholerae: structure, unfolding, and virstatin binding. Biochemistry 50(14):2962–2972
53. Saptarshi SR, Duschl A, Lopata AL (2013) Interaction of nanoparticles with proteins: relation to bio-reactivity of the nanoparticle. J Nanobiotechnology 11:26
54. De Jong WH, Borm PJ (2008) Drug delivery and nanoparticles: applications and hazards. Int J Nanomedicine 3(2):133–149
55. Ansar SM, Perera GS, Gomez P, Salomon G, Vasquez ES, Chu IW, Zou S, Pittman CU Jr, Walters KB, Zhang D (2013) Mechanistic study of continuous reactive aromatic organothiol adsorption onto silver nanoparticles. J Phys Chem C 117(51):27146–27154
56. Gadogbe M, Ansar SM, Chu IW, Zou S, Zhang D (2014) Comparative study of the self-assembly of gold and silver nanoparticles onto thiophene oil. Langmuir 30:11520–11527
57. Herrera GM, Padilla AC, Hernandez-Rivera SP (2013) Surface enhanced Raman scattering (SERS) studies of gold and silver nanoparticles prepared by laser ablation. Nanomaterials 3(1):158–172
58. Ghosh D, Chattopadhyay N (2013) Gold nanoparticles: acceptors for efficient energy transfer from the photoexcited fluorophores. Optics and Photonics Journal 3:18–26. https://doi.org/10.4236/opj.2013.31004
59. Haes AJ, Zou S, Schatz GC, Van Duyne RP (2004) Nanoscale optical biosensor: short range distance dependence of the localized surface plasmon resonance of noble metal nanoparticles. J Phys Chem B 108(22):6961–6968
60. Mirkin CA, Letsinger RL, Mucic RC, Storhoff JJ (1996) A DNA-based method for rationally assembling nanoparticles into macroscopic materials. Nature 382:607–609
61. Andrews DL, Demidov AD (eds) (1999) Resonance energy transfer. Wiley, England
62. Bogdan M, Pirnau A, Floare C, Bugeac C (2008) Binding interaction of indomethacin with human serum albumin. J Pharm Biomed Anal 47(4–5):981–984
63. Mitchell JA, Whitfield JH, Zhang WH, Henneberger C, Janovjak H, O'Mara ML, Jackson CJ (2016) Rangefinder: a semisynthetic FRET sensor design algorithm. ACS Sensors 1(11):1286–1290
64. Ghosh D, Girigoswami A, Chattopadhyay N (2012) Superquenching of coumarin 153 by gold nanoparticles. J Photochem Photobiol A Chem 242:44–50
65. Navarro JR, Werts MH (2013) Resonant light scattering spectroscopy of gold, silver and gold–silver alloy nanoparticles and optical detection in microfluidic channels. Analyst 138:583–592
66. Röcker C, Pötzl M, Zhang F, Parak WJ, Nienhaus GU (2009) A quantitative fluorescence study of protein monolayer formation on colloidal nanoparticles. Nat Nanotechnol 4:577–580

67. Lacerda SHDP, Park JJ, Meuse C, Pristinski D, Becker ML, Karim A, Douglas JF (2009) Interaction of gold nanoparticles with common human blood proteins. ACS Nano 4(1):365–379
68. Boulos SP, Davis TA, Yang JA, Lohse SE, Alkilany AM, Holland LA, Murphy CJ (2013) Nanoparticle–protein interactions: a thermodynamic and kinetic study of the adsorption of bovine serum albumin to gold nanoparticle surfaces. Langmuir 29(48):14984–14996
69. Brewer SH, Glomm WR, Johnson MC, Knag MK, Franzen S (2005) Probing BSA binding to citrate-coated gold nanoparticles and surfaces. Langmuir 21(20):9303–9307
70. De-Llanos R, Sánchez-Cortes S, Domingo C, García-Ramos JV, Sevilla P (2011) Surface plasmon effects on the binding of antitumoral drug emodin to bovine serum albumin. J Phys Chem C 115(25):12419–12429
71. Dasgupta N, Ranjan S, Patra D, Srivastava P, Kumar A, Ramalingam C (2016) Bovine serum albumin interacts with silver nanoparticles with a "side-on" or "end on" conformation. Chem Biol Interact 253:100–111
72. Wang G, Lu Y, Hou H, Liu Y (2017) Probing the binding behavior and kinetics of silver nanoparticles with bovine serum albumin. RSC Adv 7:9393–9401
73. Mariam J, Dongre PM, Kothari DC (2011) Study of interaction of silver nanoparticles with bovine serum albumin using fluorescence spectroscopy. J Fluoresc 21:2193–2199
74. Yu S, Perálvarez-Marín A, Minelli C, Faraudo J, Roig A, Laromaine A (2016) Albumin-coated SPIONs: an experimental and theoretical evaluation of protein conformation, binding affinity and competition with serum proteins. Nanoscale 8:14393–14405
75. Rezwan K, Meier LP, Rezwan M, Vörös J, Textor M, Gauckler LJ (2004) Bovine serum albumin adsorption onto colloidal Al_2O_3 particles: a new model based on zeta potential and UV−Vis measurements. Langmuir 20(23):10055–10061
76. Jennings TL, Singh MP, Strouse GF (2006) Fluorescent lifetime quenching near d = 1.5 nm gold nanoparticles: probing NSET validity. J Am Chem Soc 128(16):5462–5467
77. Sen T, Sadhu S, Patra A (2007) Surface energy transfer from rhodamine 6G to gold nanoparticles: a spectroscopic ruler. Appl Phys Lett 91(4):043104